This version of the ESI replaces the one published on 4th May 2022 to correct some data in the tables

Supporting Information

Optical Absorption and Shape Transition in Neutral Sn_N Clusters with $N \leq 40$: A Photodissociation Spectroscopy and Electric Beam Deflection Study

Andreas Lehr,* Filip Rivic, Marc Jäger, Martin Gleditzsch, and Rolf Schäfer

Eduard-Zintl-Institut, Technical University of Darmstadt, Alarich-Weiss-Straße 8, 64287 Darmstadt, Germany

---

1. Cationic Sn_N^+ Clusters with $N = 6 - 20, 25, 30, 40$

Not only have the neutral Sn_N clusters been studied, but also the cationic species Sn_N^+ were investigated theoretically (cf. Fig. S1). The same independent procedure for finding structures has been applied based on a Genetic Algorithm and a subsequent reoptimization of structural candidates at the PBE0/cc-pVTZ-PP and LC-ωPBEh/def2-TZVPP level of theory plus performing single-point calculations at the CCSD(T)/cc-pVTZ-PP level of theory (for details see manuscript). Whereas the local minimum structures of the neutral clusters were all spin singlets, the cationic clusters were all found to be spin doublets, thus being potentially subject to Jahn-Teller stabilization, whenever a doubly-degenerate configuration is found for the ground state. This results in oftentimes distorted geometries with lower symmetries compared to the neutral clusters and an overall larger variety in structural candidates. Hence, it has been found favorable to reoptimize neutral clusters or fill the pool of the Genetic Algorithm based on cationic structures which were not detected in the investigation of their neutral counterparts. While many of the cationic isomers appear to be transition states in the neutral clusters, some other neutral clusters could only be identified by this approach.

2. Vibrational Frequencies and Temperature

Calculating the vibrational frequencies allows for checking whether reoptimized structures truly correspond to local minima on the potential energy surface. Furthermore, the cluster's vibrational modes being thermally excited in the experiments might have a significant impact on the recorded electric deflection profiles and photodissociation spectra. At 300 K roughly all vibrational modes can be expected to be excited, whereas at 16 K almost only the largest clusters under study have vibrational modes low enough in energy to be thermally excited (cf. Fig. S2). It has been shown in previous investigations that down to nozzle temperatures of $30 - 50$ K, the vibrational temperature is observed to behave accordingly.[2,3] In the photodissociation experiments vibrational finestructure is not resolved, but certain differences in, i.e., the degree of hot band contributions are expected to alter the general course of the absorption spectrum slightly. Here, we lowered the nozzle temperature in order to shift the contributions of participating structural isomers in the molecular beam. Thermal excitation of vibrational modes in the electric deflection experiment can lead to a reduction in broadening of the molecular beam. This is due to the electric dipole moment being quenched as a result of the non-rigidity of the clusters upon vibrational excitation and is discussed as possibility for the largest clusters.

3. Boltzmann Correction for Structural Isomer Mixtures

The clusters Sn_8, Sn_{11}, Sn_{12} and Sn_{19} all indicate the presence of more than one structural isomer in the molecular beam both in the electric deflection experiment at 16 K as well as the photodissociation experiments at 32 K and 300 K. The ratios or isomer mixtures obtained from simply fitting the classical trajectory simulations and TDDFT absorption spectra to the experimental deflection profile and photodissociation spectrum do not always give the most physical result. Taken the Sn_8 cluster as an example, a mixture of 40 : 60 of isomers 8-I : 8-II is estimated at 300 K from comparing the course of the experimental photodissociation spectrum with the TDDFT predicted absorption spectra (cf. Fig. S3). The Boltzmann law determines a maximum mixture of 50 : 50 for large temperatures when taking into account the slight distortion of isomer 8-II from D_{2h} symmetry and thus assuming equal symmetry factors.

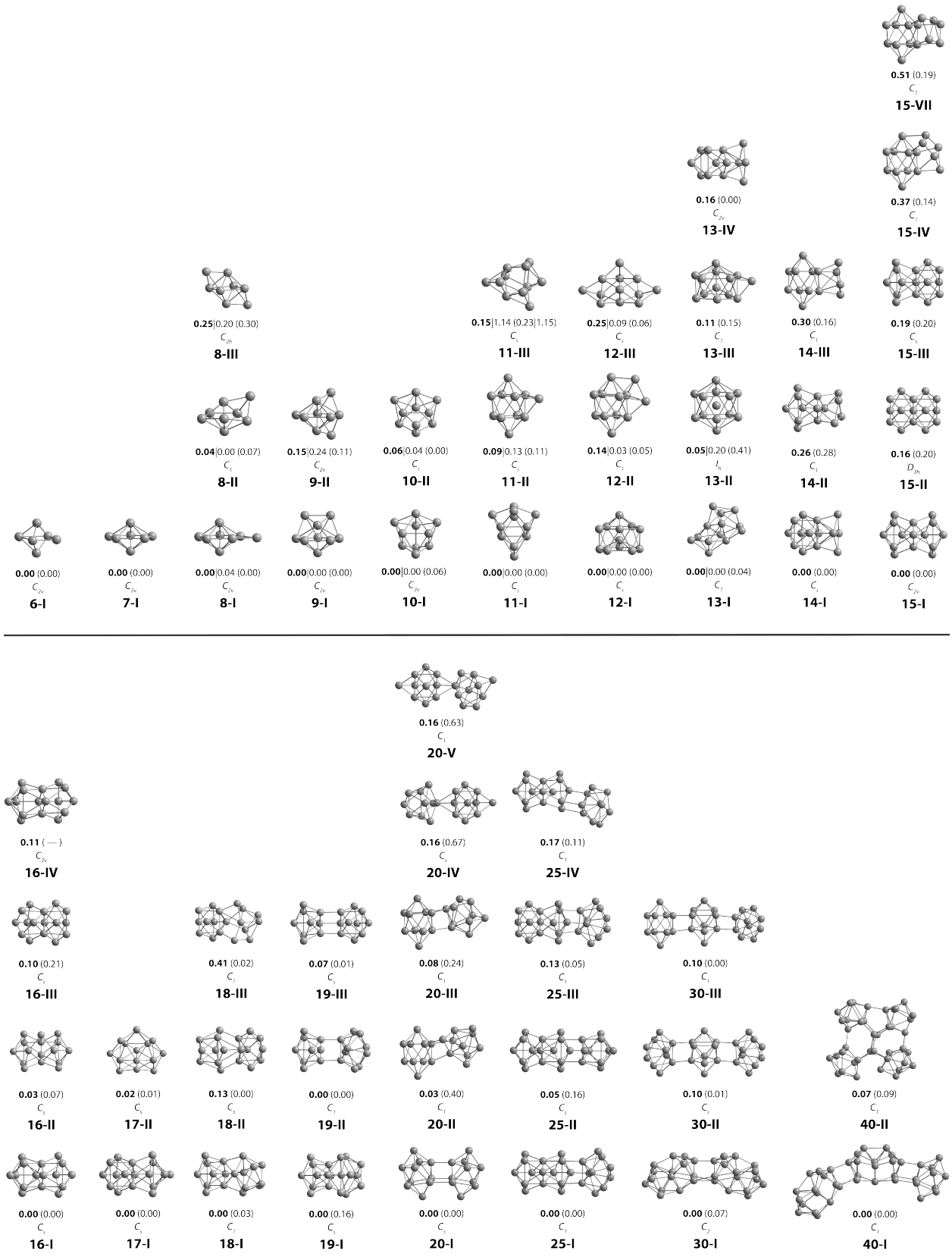

Figure S1. Summary of the Sn_N^+ structural isomers shown together with their molecular point groups and energies ΔE relative to the GM in eV optimized at the PBE0/cc-pVTZ-PP|CCSD(T)/cc-pVTZ-PP(LC-ωPBEh/def2-TZVPP) levels of theory. For Sn_{30}^+ and Sn_{40}^+ the structures were obtained from reoptimizing low-lying isomers of the neutral Sn_N species.

Table S1. Ellipsoid semiaxes A_1, A_2 and A_3 in Å and the dimensionless relative quantities A_1^{rel}, A_2^{rel} and A_3^{rel} as a measure for the cluster isomer's prolateness (from approximately Sn_{12} onward, $A_1^{\mathrm{rel}} > A_2^{\mathrm{rel}} \approx A_3^{\mathrm{rel}}$). In contradiction, the isomer 40-II has a clear oblate shape ($A_1^{\mathrm{rel}} \approx A_2^{\mathrm{rel}} > A_3^{\mathrm{rel}}$). The moment of inertia tensor components I_{ii} with $i = x, y, z$ can be taken from Tab. S3.

Isomer	A_1 / Å	A_2 / Å	A_3 / Å	A_1^{rel}	A_2^{rel}	A_3^{rel}
6-I	3.04	3.04	2.20	1.10	1.10	0.80
7-I	3.45	3.44	1.90	1.18	1.18	0.65
8-I	3.94	3.13	2.52	1.23	0.98	0.79
8-II	4.56	2.76	2.34	1.42	0.86	0.73
9-I	4.10	3.41	2.53	1.23	1.02	0.75
9-II	3.97	3.14	3.06	1.17	0.93	0.90
10-I	3.60	3.44	3.44	1.03	0.98	0.98
11-I	4.15	3.70	3.15	1.13	1.01	0.86
11-II	4.42	3.45	3.25	1.19	0.93	0.88
11-III	4.22	3.57	3.25	1.15	0.97	0.88
11-IV	4.14	3.64	3.24	1.13	0.99	0.88
12-I	5.41	3.17	3.06	1.39	0.82	0.79
12-II	3.99	3.99	3.27	1.06	1.06	0.87
12-III	4.74	3.80	2.95	1.24	0.99	0.77
13-I	5.14	3.49	3.31	1.29	0.88	0.83
13-II	5.36	3.41	3.28	1.33	0.85	0.82
14-I	5.30	3.56	3.44	1.29	0.87	0.84
15-I	5.21	3.70	3.69	1.24	0.88	0.88
15-II	5.55	3.73	3.39	1.31	0.88	0.80
15-III	5.01	3.74	3.74	1.20	0.90	0.90
16-I	5.67	3.93	3.48	1.30	0.90	0.80
17-I	6.14	4.02	3.45	1.35	0.89	0.76
17-II	5.26	4.43	3.64	1.18	1.00	0.82
18-I	6.91	3.63	3.61	1.47	0.77	0.77
18-II	6.64	3.71	3.71	1.42	0.79	0.79
19-I	7.74	3.79	3.43	1.55	0.76	0.69
19-II	6.75	3.78	3.78	1.41	0.79	0.79
19-III	7.75	3.86	3.44	1.54	0.77	0.69
20-I	8.04	4.12	3.32	1.56	0.80	0.64
20-II	8.62	3.44	3.43	1.67	0.67	0.66
20-III	8.35	3.82	3.45	1.60	0.73	0.66
20-IV	8.67	3.48	3.44	1.67	0.67	0.66
20-V	8.40	3.81	3.40	1.61	0.73	0.65
25-I	10.17	3.76	3.58	1.74	0.64	0.61
25-II	10.15	3.86	3.49	1.74	0.66	0.60
25-III	9.74	3.95	3.67	1.68	0.68	0.63
30-I	12.46	4.12	3.44	1.87	0.62	0.52
30-II	12.46	3.88	3.72	1.86	0.58	0.56
30-III	11.70	4.04	3.70	1.81	0.62	0.57
40-I	15.36	5.09	3.63	1.91	0.63	0.45
40-II	8.83	8.05	3.79	1.28	1.17	0.55

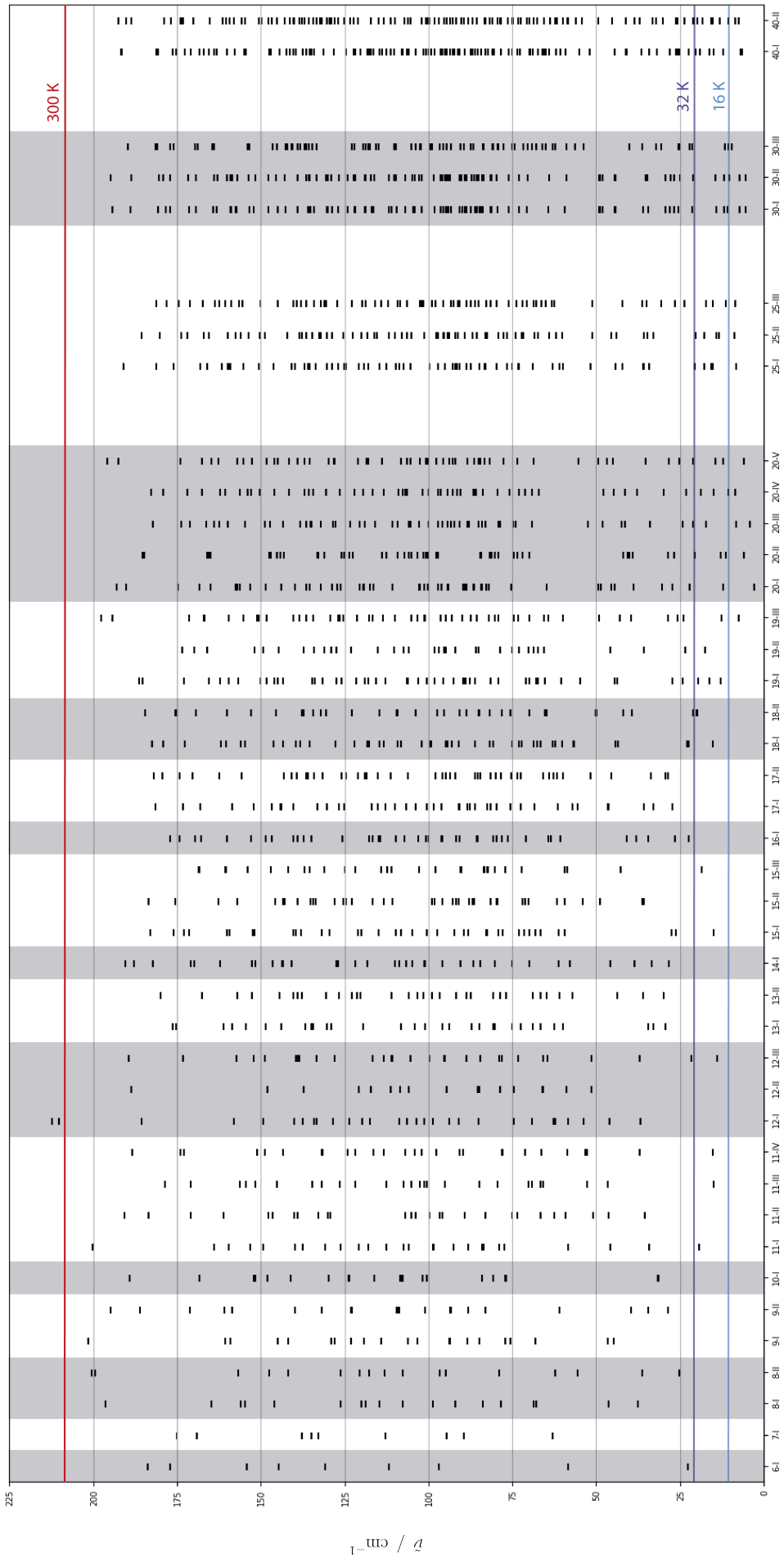

Figure S2. Vibrational Frequencies $\tilde{\nu}$ of all Sn_N structural isomers calculated at the PBE0/cc-pVTZ-PP level of theory. The wavenumbers corresponding to the experimental temperatures 300 K, 32 K and 16 K are highlighted by horizontal lines.

Table S2. Dissociation energies E_D in eV, calculated for the energetically most favorable fragmentation channels and estimated from experimental atomization enthalpies [1], together with the excess energies $E - E_D$ in eV for all structural isomers computed via the RRKM theory at a lifetime ($\hat{=}$ experimental flight time) of $\tau = 100\,\mu$s. The vibrational frequencies can be found in Fig. S2. The experimental dissociation energy given in a round bracket refers to a falsely assumed cluster geometry and has to be viewed with care. [1] The excess energies given in square brackets correspond to RRKM results based on the experimental dissociation energies.

		Theory		**Experiment**
Isomer	Fragmentation	E_D / eV	$E - E_D$ / eV ($\tau = 100\,\mu$s)	E_D / eV
2-I	$Sn_2 \rightarrow Sn + Sn$	2.18	–	1.90
3-I	$Sn_3 \rightarrow Sn_2 + Sn$	2.91	0.00 [0.00]	(3.06)
4-I	$Sn_4 \rightarrow Sn_3 + Sn$	3.61	0.03 [0.03]	3.59
5-I	$Sn_5 \rightarrow Sn_4 + Sn$	3.05	0.22 [0.17]	2.49
6-I	$Sn_6 \rightarrow Sn_5 + Sn$	3.53	0.62 [0.66]	3.73
7-I	$Sn_7 \rightarrow Sn_6 + Sn$	3.47	1.02 [0.88]	3.06
8-I	$Sn_8 \rightarrow Sn_7 + Sn$	2.06	0.84	
8-II		1.88	0.75	
9-I	$Sn_9 \rightarrow Sn_7 + Sn_2$	3.25	1.71	
9-II		3.01	1.38	
10-I	$Sn_{10} \rightarrow Sn_9 + Sn$	3.33	2.32	
11-I	$Sn_{11} \rightarrow Sn_{10} + Sn$	2.12	1.72	
11-II		2.11	1.71	
11-III		2.03	1.65	
11-IV		2.01	1.63	
12-I	$Sn_{12} \rightarrow Sn_6 + Sn_6$	1.85	1.73	
12-II		1.83	1.72	
12-III		1.71	1.60	
13-I	$Sn_{13} \rightarrow Sn_7 + Sn_6$	1.26	1.30	
13-II		1.22	1.26	
14-I	$Sn_{14} \rightarrow Sn_7 + Sn_7$	1.02	0.97	
15-I	$Sn_{15} \rightarrow Sn_8 + Sn_7$	1.89	2.47	
15-II		1.86	2.54	
15-III		1.86	2.54	
16-I	$Sn_{16} \rightarrow Sn_9 + Sn_7$	1.39	2.03	
17-I	$Sn_{17} \rightarrow Sn_{10} + Sn_7$	0.75	2.69	
17-II		0.57	0.78	
18-I	$Sn_{18} \rightarrow Sn_{11} + Sn_7$	1.59	2.81	
18-II		1.41	2.47	
19-I	$Sn_{19} \rightarrow Sn_{10} + Sn_9$	0.90	1.48	
19-II		0.83	1.46	
19-III		0.81	1.41	
20-I	$Sn_{20} \rightarrow Sn_{10} + Sn_{10}$	0.58	0.85	
20-II		0.52	0.88	
20-III		0.51	0.86	
20-IV		0.47	0.77	
20-V		0.46	0.74	
25-I	$Sn_{25} \rightarrow Sn_{15} + Sn_{10}$	0.96	2.50	
25-II		0.95	2.46	
25-III		0.88	2.25	
30-I	$Sn_{30} \rightarrow Sn_{20} + Sn_{10}$	1.07	3.57	
30-II		1.06	3.53	
30-III		0.92	3.02	
40-I	$Sn_{40} \rightarrow Sn_{30} + Sn_{10}$	1.00	4.51	
40-II		0.94	4.34	

Hence, the isomer mixture of the TDDFT spectra is corrected accordingly to give a physically more reasonable fit. Adjusting the isomer mixtures in the trajectory simulations and TDDFT spectra a little does not alter the resulting simulations to a huge extent which is why we believe this combined approach will yield the best results. A similar technique is applied for the clusters Sn_{11} and Sn_{19}. In the latter case a fit of reversed slope is obtained, indicating that the energetic order of the isomers is not well represented at the given levels of theory. The Sn_{12} cluster does not show a change in isomer mixture over the temperature range studied, implying that both isomers are energetically equal.

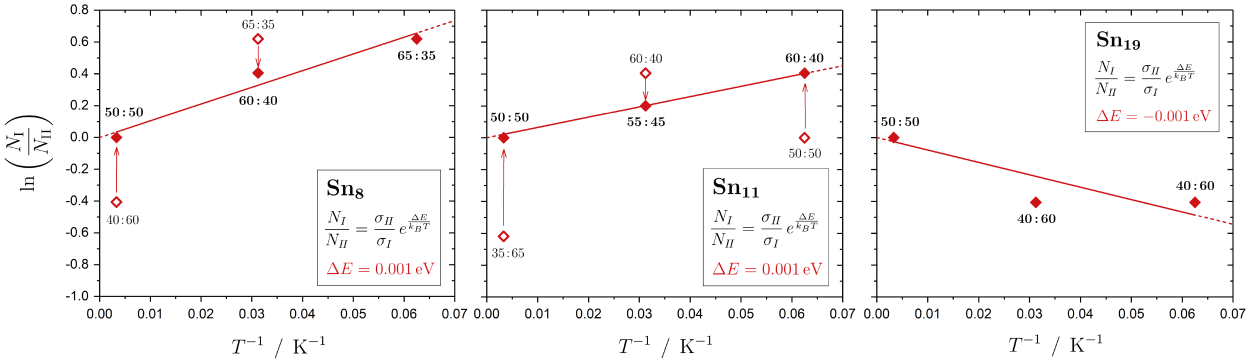

Figure S3. Boltzmann fit and correction of the isomer mixtures observed in the experimental electric beam deflection (at 16 K) and photodissociation spectroscopy experiments (at 32 K and 300 K) for the clusters Sn_8, Sn_{11} and Sn_{19}. The isomer ratios N_I/N_{II} directly obtained from comparing experimental data with theoretical simulations (empty diamonds) are corrected in order to yield a better agreement with the Boltzmann law considering molecular symmetry factors σ (filled diamonds).

4. Electric Deflection Profiles:
Impact of Electric Dipole Moment and Rotational Temperature

To investigate the influence of the dipole moment and the rotational temperature on the resulting simulated deflection profile, we varied those parameters for the trajectory simulations of the Sn_{10} deflection profile with a nozzle temperature of 16 K and a deflection voltage of 24 kV. This cluster is chosen, since only one structural isomer is forecasted by quantum chemical calculations in the considered energy range which additionally possesses only one non-zero component of the calculated electric dipole moment. The resulting deflection profiles are shown in Fig. S4. Since the initial simulation overestimates the broadening of the molecular beam slightly, only an increase of the electric dipole moment component and a decrease of the rotational temperature is considered. The decreasing of the electric dipole moment of about 20 % alone results in a deflection profile with lesser broadening but it overestimates the intensities at around 0.2 D and fails to describe the intensity at higher deflection $\geq$ 0.6 D properly. When only increasing the rotational temperature the resulting deflection profile is less broadened and, therefore, describes the experimental data to a good approximation. However, the difference from the initial deflection profile is marginal. By changing both parameters at the same time, the resulting deflection profile intensity at the center increases slightly and the intensity at higher deflection is still described to a good approximation. As to be assumed, the difference to the initial simulated deflection profile is now bigger. However, in conclusion all shown simulated deflection profiles describe the experimental data to a good approximation qualitatively so that there is a certain freedom in choosing these two parameters.

5. Comparison of Electric Dipole Moments and Polarizabilities

In Tab. S3 the dielectric properties of all Sn_N structural isomers both computed quantum chemically and extracted from the experimental data are summarized. The latter are calculated by perturbation analysis. Note that this approach is only valid as long as the rotational energy of the clusters is much higher than its interaction with the electric field ($k_B T_{rot} \gg \mu E_z$). This requirement holds even for the cluster with the highest computed electric dipole

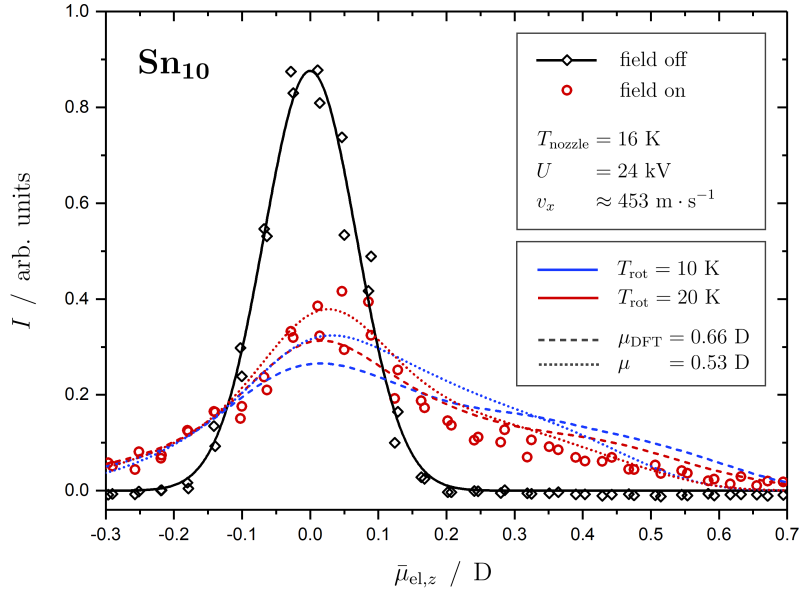

Figure S4. Electric beam deflection profiles, given as arbitrary normalized intensity I as a function of the mean projection of the dipole moment on the field direction $\bar{\mu}_{\mathrm{el},z}$, are shown with (red circles) and without applied electric field (black diamonds). The latter one has been fitted by a Gaussian around the center of deflection (solid black line). The electric deflection profiles were recorded at lowest possible nozzle temperatures of 16 K for the Sn_{10} cluster, a deflection voltage of 24 kV and velocities of 453 $\mathrm{m\,s^{-1}}$. The simulated deflection profiles (dashed lines) are shown for rotational temperatures of $T_{\mathrm{rot}} = 10$ K and 20 K as well as the computed electric dipole moment μ_{DFT} at the PBE0/cc-pVTZ-PP level of theory and an electric dipole moment μ decreased by 20 %.

moment of 2.8 D (isomer 19-II). By assuming that the clusters are spherical and rigid in the electric field, the electric polarizability $\alpha_{\mathrm{iso}}^{\mathrm{exp}}$ is derived from the shift of the two adapted Gaussian functions for the data points with and without applied electric field. The electric dipole moment $\mu_{\mathrm{iso}}^{\mathrm{exp}}$ is calculated via the change in their variance.[4,5] The given absolute deviations result from the error of the Gaussian fits and the velocities with about 3 %.[3,6] The electric polarizabilities extracted from the experiment are overestimated by a factor of $2-3$ for most of the clusters. This is due to a contribution of the electric dipole moment to the purely electronic polarizability which originates from an adiabatic polarization process.[4] Thus, the experimental polarizabilities can be regarded as upper limits to the purely electronic polarizability. By using second-order perturbation theory the effective polarizability α_{eff} can be written as follows.

$$\alpha_{\mathrm{eff}} = \alpha_{\mathrm{iso}} + \frac{2}{9}\frac{\left(\mu_{\mathrm{iso}}^{\mathrm{exp}}\right)^2}{k_{\mathrm{B}}T_{\mathrm{rot}}} \tag{1}$$

Assuming a rotational temperature of $T_{\mathrm{rot}} = 20$ K, inserting the calculated electric polarizabilities α_{iso} as a reference and treating the correction via the experimentally extracted electric dipole moments $\mu_{\mathrm{iso}}^{\mathrm{exp}}$, the effective polarizabilities for all structural isomers can be determined. For most of the clusters the effective polarizabilities are now matching better with the extracted polarizabilities within a maximum error of 20 % which is the deviation assumed for the DFT calculations. It should be mentioned that for the Sn_N clusters with $N = 10, 11, 12, 19$ and 25, the experimental data with applied electric field cannot be properly described by a single Gaussian function. Thus, the extraction of the dielectric properties is not conceivable for these clusters and yields much larger electric polarizabilities with greater errors. Additionally, it is to be noted that the errors of the data extracted for the clusters with $N > 18$, except for Sn_{20}, are in general larger than for the smaller clusters. This can be traced back to two reasons. First, the data for the larger clusters are recorded at a nozzle temperature of 30 K and the clusters are, consequently, slightly faster. The corresponding contribution to the errors of the polarizability and electric dipole moment are for this reason greater. Second, the measured data are more scattered due to lower mass signal intensities which is why the error is larger in general. Nevertheless, the errors for the effective polarizability do not exceed 12 % (for isomer 19-II).

Table S3. Summary of geometric and dielectric properties obtained at the PBE0/cc-pVTZ-PP level of theory and deduced from the electric beam deflection experiment at 24 kV for Sn_N clusters with $N < 19$ and 20 kV for $N \geq 19$. The properties comprise the moment of inertia tensor components I_{xx}, I_{yy} and I_{zz}, the electric dipole moment vector components μ_x, μ_y and μ_z as well as the isotropic value $\mu_{\mathrm{iso}}^{(\mathrm{exp})}$ and the isotropic and effective electric polarizabilities $\alpha_{\mathrm{iso}}^{(\mathrm{exp})}$ and α_{eff}.

	Theory								Experiment		
Isomer	I_{xx} / u Å^2	I_{yy} / u Å^2	I_{zz} / u Å^2	μ_x / D	μ_y / D	μ_z / D	μ_{iso} / D	α_{iso} / Å^3	$\mu_{\mathrm{iso}}^{\mathrm{exp}}$ / D	$\alpha_{\mathrm{iso}}^{\mathrm{exp}}$ / Å^3	α_{eff} / Å^3
6-I	2,004.50	2,004.50	2,629.34	0.00	0.00	0.00	0.00	43.25	0.07±0.00	56.31± 6.96	43.66± 0.02
7-I	2,571.34	2,571.39	3,944.76	0.00	0.00	0.00	0.00	49.42	0.04±0.00	38.89± 4.70	49.56± 0.01
8-I	3,067.97	4,160.57	4,812.76	0.28	0.00	-0.51	0.59	58.05	0.22±0.00	39.88± 5.49	61.94± 0.08
8-II	2,485.59	4,990.21	5,403.73	0.00	0.00	0.00	0.00	59.51			63.41± 0.08
9-I	3,855.51	4,965.05	6,089.89	0.00	0.00	-0.23	0.23	64.14	0.16±0.00	57.24± 4.69	66.13± 0.04
9-II	4,104.95	5,355.76	5,468.95	0.23	0.00	0.00	0.23	64.26			66.25± 0.04
10-I	5,613.51	5,890.34	5,890.44	-0.66	0.00	0.00	0.66	69.87	0.48±0.01	74.70±11.54	88.29± 0.72
11-I	6,170.30	7,079.76	8,077.62	1.39	-0.85	0.00	1.63	77.71	0.63±0.02	170.04±17.22	109.74± 1.88
11-II	5,879.55	7,865.18	8,219.67	0.44	0.31	0.00	0.54	79.21			111.24± 1.88
11-III	6,086.62	7,409.91	7,981.19	1.13	-0.16	0.00	1.14	78.13			110.16± 1.88
11-IV	6,191.30	7,217.38	7,936.70	1.35	0.00	0.08	1.35	77.97			110.00± 1.88
12-I	5,548.11	11,017.54	11,213.18	0.00	-0.12	0.00	0.12	89.32	0.46±0.01	122.62±14.46	106.50± 0.88
12-II	7,586.28	7,586.63	9,071.35	0.00	0.00	0.19	0.19	83.53			100.71± 0.88
12-III	6,591.91	8,876.77	10,515.52	-2.17	-0.84	0.00	2.33	86.07			103.25± 0.88
13-I	7,143.67	11,536.04	11,913.23	-0.56	0.00	0.00	0.56	94.90	0.53±0.01	102.56±15.37	117.48± 1.19
13-II	6,924.42	12,190.42	12,462.81	-0.72	-0.02	-0.23	0.75	93.82			116.40± 1.19
14-I	8,162.34	13,292.71	13,568.86	-0.98	-0.40	0.00	1.05	99.73	0.54±0.02	123.93±18.26	123.23± 1.51
15-I	9,723.35	14,543.42	14,545.35	0.27	0.00	-0.15	0.31	107.40	0.21±0.01	104.10± 9.56	110.80± 0.17
15-II	9,044.81	15,086.15	15,933.17	0.00	0.00	-0.04	0.04	108.47			111.87± 0.17
15-III	9,978.14	13,917.01	13,917.05	0.00	0.00	0.00	0.00	105.63			109.02± 0.17
16-I	10,461.39	16,803.04	18,064.60	0.00	0.85	0.00	0.85	115.27	0.31±0.01	114.60±12.11	123.03± 0.40
17-I	11,318.42	20,036.61	21,734.53	-0.36	0.17	0.00	0.39	125.85	0.27±0.01	124.39±13.27	131.71± 0.38
17-II	13,283.99	16,519.74	19,109.36	0.00	0.79	-0.47	0.92	122.12			127.98± 0.38
18-I	11,199.20	25,988.17	26,025.78	0.00	0.14	0.00	0.14	138.17	0.13±0.01	122.05±10.63	139.54± 0.13
18-II	11,732.82	24,733.62	24,733.76	2.03	0.00	0.00	2.03	133.77			150.51± 0.13
19-I	11,778.93	32,391.28	33,546.44	-1.83	0.29	0.00	1.85	152.28	1.77±0.17	383.52±43.23	405.18±47.65
19-II	12,906.08	26,994.65	26,994.71	2.78	0.00	0.00	2.78	140.86			393.76±47.65
19-III	12,067.23	32,441.65	33,832.38	-1.03	0.01	-0.15	1.04	149.84			402.74±47.65
20-I	13,293.03	35,943.72	38,765.02	0.00	0.00	0.00	0.00	157.15	0.49±0.04	259.78±24.06	176.21± 2.87
20-II	11,199.79	40,835.47	40,892.98	0.00	0.00	-0.06	0.06	163.73			182.79± 2.87
20-III	12,597.36	38,784.06	40,047.64	1.12	-0.12	-0.47	1.22	161.05			180.11± 2.87
20-IV	11,367.76	41,266.63	41,416.62	-0.11	0.51	-0.19	0.56	159.57			178.63± 2.87
20-V	12,407.61	39,016.85	40,418.53	0.21	0.14	0.00	0.25	158.79			177.85± 2.87
25-I	15,982.97	69,024.13	69,790.59	-0.71	2.25	0.00	2.36	216.01	1.63±0.15	454.48±41.96	431.43±39.06
25-II	16,043.53	68,363.48	69,984.73	-1.93	0.03	0.44	1.98	216.79			428.15±39.06
25-III	17,244.60	64,280.73	65,532.63	0.58	-0.35	0.56	0.88	213.51			432.48±39.06
30-I	20,522.20	119,052.44	122,716.44	0.00	0.55	0.25	0.60	274.28	1.10±0.08	520.02±31.30	372.60±15.02
30-II	20,593.40	120,421.93	121,280.50	-0.09	0.45	-0.27	0.53	274.44			372.76±15.02
30-III	21,383.27	107,203.68	109,112.14	0.18	-1.48	0.00	1.49	282.27			380.59±15.02
40-I	37,071.99	236,543.42	248,616.14	1.10	-2.23	-0.04	2.49	428.22	1.62±0.17	789.44±44.06	641.11±43.80
40-II	75,235.65	87,689.99	135,655.74	-1.59	-0.80	-0.04	1.78	339.59			552.48±43.80

6. Fundamental and Optical TDDFT Band Gaps

The photodissociation spectrum corresponds to the true one-photon absorption spectrum when there are no non-dissociative pathways following the light absorption and the excitation energy is above the dissociation threshold considering the corresponding lifetime under experimental conditions. These requirements often impede the determination of optical band gaps from the low-energy region of the spectrum. Thus, fundamental and „optical“ band gaps were extracted from TDDFT results (cf. Fig. S5). Due to the increasing overall light absorption with cluster size, the optical band gaps approach the fundamental ones over this course. The band gaps of the largest clusters are still significantly above the bulk value for the zero-gap semiconducting α-Sn indicating the structural differences that are still present at this cluster size.

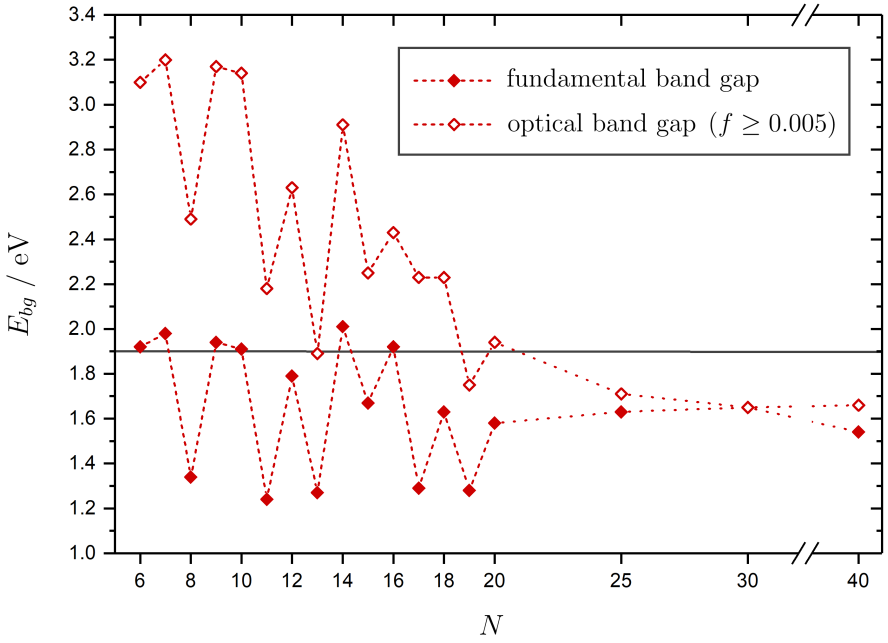

Figure S5. Fundamental HOMO-LUMO and „optical“ band gaps with oscillator strengths $f \geq 0.005$ of the Sn_N clusters at the LC-ωPBEh/def2-TZVPP level of theory averaged over the isomers which were identified to be present in the experiment. The horizontal line at 1.9 eV gives the smallest accessible single-photon energy available in the photodissociation spectroscopy experiment.

References

[1] G. Meloni, R. W. Schmude, J. E. Kingcade, K. A. Gingerich, *J. Chem. Phys.* **2000**, *113*, 1852–1856.

[2] U. Rohrmann, R. Schäfer, *Phys. Rev. Lett.* **2013**, *111*, 133401.

[3] T. M. Fuchs, F. Rivic, R. Schäfer, *Phys. Rev. A* **2021**, *104*, 012820.

[4] S. Schäfer, B. Assadollahzadeh, M. Mehring, P. Schwerdtfeger, R. Schäfer, *J. Phys. Chem. A* **2008**, *112*, 12312–12319.

[5] S. Heiles, R. Schäfer, *Dielectric Properties of Isolated Clusters: Beam Deflection Studies*, Springer, Heidelberg, **2014**.

[6] U. Rohrmann, S. Schäfer, R. Schäfer, *J. Phys. Chem. A* **2009**, *113*, 12115–12121.